Spring-neap modulation of internal tide mixing and vertical nitrate fluxes at a shelf edge in summer.

Jonathan Sharples[1], Jacqueline F. Tweddle[2], J. A. Mattias Green[3], Matthew R. Palmer[3], Young-Nam Kim[2], Anna E. Hickman[2], Patrick M. Holligan[2], C. Mark Moore[4], Tom P. Rippeth[3], John H. Simpson[3], and Vladimir Krivtsov[3]

[1] Proudman Oceanographic Laboratory, 6 Brownlow Street, Liverpool, L3 5DA, United Kingdom

[2] National Oceanography Centre, Empress Dock, Southampton, SO14 3ZH, United Kingdom

[3] School of Ocean Sciences, University of Wales Bangor, Menai Bridge, Gwynedd, LL59 5EY, United Kingdom

[4] Department of Biological Sciences, University of Essex, Colchester, CO4 3SQ, United Kingdom

Corresponding author:
Jonathan Sharples
j.sharples@pol.ac.uk
tel: +44 151 795 4800
fax: +44 151 795 4801

Running Head: Nitrate fluxes at a shelf edge

Article published: *Limnology and Oceanography*, **52(5)**, 1735-1747, 2007.
Available online at: http://aslo.org/lo/toc/vol_52/issue_5/1735.pdf

Acknowledgements

This work was supported by the UK Natural Environment Research Council (grant NER/A/S/2001/00449 (University of Southampton), NER/A/S/2001/00961 (University of Wales, Bangor), NERC core funding of the Proudman Oceanographic Laboratory), and the Defence Science and Technology Laboratory. Our thanks to the crew of the RRS *Charles Darwin* (cruise CD173) and the technical staff of the UK National Marine Facilities. We are grateful for the constructive comments from two anonymous reviewers, which helped improve this paper.

Abstract

Measurements of the intra-tidal and spring-neap variation in the vertical flux of nitrate into the base of the sub-surface chlorophyll maximum (SCM) were made at the shelf edge of the Celtic Sea, a region with strong internal mixing driven by an internal tide. The neap tide daily mean nitrate flux was 1.3 (0.9 – 1.8, 95% confidence interval) mmol m^{-2} d^{-1}. The spring tide flux was initially estimated as 3.5 (2.3 – 5.2, 95% confidence interval) mmol m^{-2} d^{-1}. The higher spring tide nitrate flux was the result of turbulent dissipation occurring within the base of the SCM, compared to deeper dissipation during neap tides, and was dominated by short events associated with the passage of internal solitons. Taking into account the likely under-sampling of these short mixing events raised the spring tide nitrate flux estimate to about 9 mmol m^{-2} d^{-1}. The neap tide nitrate flux was sufficient to support substantial new production and a considerable fraction of the observed rates of carbon fixation. Spring tide fluxes were potentially in excess of the phytoplankton community's capacity to uptake nitrate. This potential excess nitrate flux during spring tides may be utilised to support new production during the lower mixing associated with the transition towards neap tide. The shelf edge is shown to be a region with a significantly different phytoplankton community compared to the adjacent Celtic Sea and NE Atlantic Ocean, highlighting the role of gradients in physical processes leading to gradients in ecosystem structure.

Introduction

The shelf edge is an important boundary, separating the shelf seas from the open ocean. Physical processes at the shelf edge mediate the transfer of water and its constituents between the deep ocean and the shallow shelf seas (Huthnance 1995), which is of particular interest in the context of nutrient and carbon fluxes (Liu et al. 2000). Shelf edge regions have been associated with distinct biological activity, including locally enhanced growth of phytoplankton and controlling the distribution of fish larvae (Fernandez et al. 1993), to shelf edge plankton supporting marine mammals (Wishner et al. 1988) and important fisheries (Young et al. 2001). A number of species appear to use the shelf edge as a "highway" between spawning and feeding grounds (Reid 2001).

The upper shelf slope and shelf edge are often seen to be sites of enhanced internal mixing compared to the waters on either side. As the depth of the ocean changes between the open ocean and the shelf sea, the relatively steep bathymetry of the shelf slope can lead to the formation of non-linear internal (often tidal) waves, which can break into internal solitons (illustrated schematically in Fig. 1). The propagation of these solitons can lead to significant fluxes across the shelf edge (Baines 1982; Inall et al. 2001), while the current shear associated with them causes localised internal turbulence and mixing (e.g., Holloway et al. 2001; Rippeth and Inall 2002; Dale et al. 2003) which ultimately dissipates the energy of the internal tide. This mixing environment has a global impact through effects on oceanic watermass properties (Huthnance 1995) and ocean heat fluxes (Garrett 2003). More locally the enhanced turbulence and mixing can affect sediment re-suspension and distributions at the shelf edge (Heathershaw et al. 1987; Puig et al. 2004) and the vertical flux of deep nutrients to the sea surface (Holligan et al. 1985; Brickman and Loder 1993; Sharples et al. 2001*a*). There is evidence that the altered structure of the water column caused by internal mixing at the shelf edge is targeted by, for instance, spawning mackerel (Bez and Rivoirard 2001).

Understanding the physics of the shelf edge is thus important, locally and globally, and in the context of sedimentology, biochemistry, and fisheries. The focus of this contribution is the enhanced vertical mixing at the shelf edge of the Celtic Sea, driven by the internal tide, and its effect on nitrate distributions. The internal tide in the region has been seen to have a peak-to-trough amplitude of over 50 m at spring tides, propagating as a decaying wave both on-shelf and into the open ocean (Pingree et al. 1984). Observations have shown direct evidence of enhanced mixing associated with the internal wave, particularly at spring tides (New and Pingree 1990), with mixing at spring tides associated with the break-up of the internal tidal wave into trains of internal solitons (Pingree and Mardell 1985). Modelling studies of the internal tide at the Celtic Sea shelf edge also suggest mixing to be

associated more with spring tides (New 1988), with trains of shelf-ward propagating internal solitons more likely to be generated at spring tides than at neap tides (Gerkema 1996). Increased surface concentrations of nitrate and chlorophyll, associated with a band of cooler water along the shelf edge, have been recognised for some time (Pingree and Mardell 1981). Considering this increase in mixing at the shelf edge, the observed enhanced chlorophyll could be the result of either locally increased growth in response to the supply of nitrate, or of mixing of the sub-surface thermocline phytoplankton population towards the surface. There is evidence supporting increased growth of phytoplankton at the shelf edge, primarily derived from observations of an increased *f*-ratio within the band of cooler, higher-nitrate water (Elskens et al. 1997; Joint et al. 2001).

Our aim is to quantify the vertical supply of nitrate driven by internal mixing at the Celtic Sea shelf break during summer. In particular we make a first assessment of the possible temporal variability in nitrate supply associated with mixing changes over the spring-neap tidal cycle. We do this by combining tidal-cycle measurements of turbulent dissipation, using a free-fall turbulence sensor, with vertical profiles of nitrate close to a spring and a neap tide. We interpret the results in the context of how the primary production at the shelf edge may respond to the spring-neap cycle in mixing and nutrient fluxes, and show how the shelf edge is a biologically important boundary between the adjacent Atlantic Ocean and Celtic Sea shelf.

Methods

Observations were carried out during the RRS *Charles Darwin* cruise CD173 in July-August 2005 in the Celtic Sea (Fig. 2A), with all measurements carried out between a neap and a spring tide typical for the region (Fig. 2B). A station at the shelf edge (48° 34.5' N, 9° 30.6' W, depth = 200 m) was chosen within the band of low temperature and high chlorophyll (Fig. 2C, D). The ship occupied this station for two 25 hour sampling periods, between 19:00 h UTC 17 July and 20:00 h UTC 18 July (neap tide), and between 03:00 h UTC 23 July and 04:00 h UTC 24 July (spring tide). The major axis of the depth-mean tidal flow was aligned approximately NE-SW, perpendicular to the general direction of the isobaths. During the neap tide sampling period the depth-mean tidal current amplitude was 0.22 m s^{-1}. Wind speeds began at about 25 km h^{-1}, increasing to 35 km h^{-1} by the end of the period. During the spring tide sampling period the depth-mean tidal current amplitude was 0.5 m s^{-1}. Winds were 20 – 25 km h^{-1} for most of the period, rising rapidly to 55 km h^{-1} between 21:00 h on the 23 July and 00:00 h on the 24 July, and maintaining 45 – 55 km h^{-1} for the remainder of the period.

A mooring was deployed at the shelf edge station between 17 July and 24 July, providing current and temperature profiles with high time resolution. Vemco minilog temperature loggers were spaced every 10 m between the seabed and 60 m below the sea surface, and every 5 m between 55 m and 15 m below the surface. A Seabird microcat was attached to the surface marker buoy. The Vemco loggers and the microcat recorded data with a 1 minute sampling interval. Two 300 kHz RDI Workhorse ADCPs were deployed, one in a frame on the seabed and the other 100m above the seabed in a streamlined SUBS buoy (Ocean Seas Instrumentation Inc.).

A Seabird 911 CTD and rosette system was used to collect vertical profiles of salinity, temperature, and chlorophyll fluorescence, with bottle samples collected for nutrient and phytoplankton pigment analysis (Table 1). The CTD was lowered at a rate of approximately 0.5 m s^{-1}, sampling at 25 Hz. The CTD temperature was accurate to within the 0.001 °C resolution of the data (based on pre-cruise and post cruise laboratory calibrations). CTD salinity was calibrated against salinity samples analysed against standard seawater on a Guildline Autosal, resulting in a measurement error in the CTD salinity data of ±0.003 (PSS78). A Chelsea Instruments Aquatracka MKIII chlorophyll fluorometer was interfaced with the CTD, and also sampled at a rate of 25 Hz. The output of the fluorometer was compared with discrete measurements of chlorophyll *a* (Chl *a*) from filtered water samples, collected during both sampling periods. Samples were taken over the whole water column, including the surface layer, SCM, and deeper water, to cover the entire range of Chl *a* concentrations (Table 1). Chl *a* in each sample was determined following the procedure of Welschmeyer (1994) using a Turner A-10 fluorometer calibrated with a Chl *a* standard (Sigma, UK) in 90% acetone. The subsequent regression (n=58, r^2=0.8) provided a calibration of the CTD fluorescence with a rms error of ±0.2 mg Chl *a* m^{-3}. Samples for flow cytometry (2 mL) were collected from within the peak of the SCM, preserved in paraformaldehyde and then immediately frozen at -80 °C for return to the laboratory. Analysis was performed using a Beckton Dickinson FACSort flow cytometer. Phytoplankton samples were also collected from the peak of the SCM and preserved in 1-2% acidic Lugols solution. The major taxa were enumerated using a Leica DMIRB light microscope. Nitrate + nitrite was analysed in samples taken from the CTD rosette (Table 1), using standard colorimetric methods (Grasshof et al. 1983) with a Skalar Autoanalyser. The detection limit was 0.1 mmol m^{-3}, with a typical measurement error (based on replicate analyses during the cruise) of ± 0.6%.

For both occupations of the shelf edge station profiles of daily primary productivity were constructed for a range of surface light conditions using information on the light-

dependent rates of carbon fixation, in situ spectral light field, and Chl *a* following methods similar to Lorenzo et al. (2004). Light-dependent rates of carbon fixation for each sampling period were obtained at four depths between the surface and base of the SCM from standard ^{14}C Photosynthesis vs. Irradiance (PE) curves adjusted to in situ light fields using measured phytoplankton absorption spectra (Moore et al. 2006). PE parameters were interpolated linearly through the water column and assumed constant throughout the day. Photoinhibition was assumed to have negligible effect on the results integrated between the sea surface and the base of the SCM. Spectral reconstruction of in situ light fields was achieved using a mean value of transmittance through the air-water interface, average in-water surface spectra, and attenuation vs. Chl *a* relationships at six wavelengths, using data obtained from a SATLANTIC profiler.

Measurements of turbulent dissipation, ε ($m^2\ s^{-3}$), were carried out using the FLY free-fall microstructure probe (Dewey et al. 1987). FLY carries two shear sensors, sampled at 274 Hz while the profiler free-falls to the seabed at a speed of 0.7 – 0.8 m s^{-1}. Subsequent analysis of the shear data to provide profiles of turbulent dissipation followed that described by Rippeth et al. (2003). FLY also carries temperature and conductivity sensors, providing vertical profiles of temperature, salinity, and density concomitant with the dissipation profiles. Profiles of vertical turbulent diffusion, K_z, can be calculated for each of the individual dissipation profiles by (Osborn 1980)

$$K_z = \Gamma \frac{\varepsilon}{N^2} \qquad (m^2\ s^{-1}) \qquad (1)$$

The factor Γ, often referred to as the mixing efficiency, is taken to be constant at 0.2. The buoyancy frequency, N (s^{-1}), can be calculated using the density profile (ρ, kg m^{-3}) measured by FLY

$$N^2 = -\frac{g}{\rho}\left(\frac{\partial \rho}{\partial z}\right) \qquad (s^{-2}) \qquad (2)$$

with g = 9.81 m s^{-2} and z the depth (metres, positive upward).

In principle the sampling method aimed at using CTD and FLY data to provide tidally-resolved estimates of vertical turbulent fluxes of nitrate, NO_3 (mmol m^{-3}), via:

$$NO_{3\,flux} = -K_z\left(\frac{\partial NO_3}{\partial z}\right) \qquad (\text{mmol } m^{-2}\ s^{-1}) \qquad (3)$$

with $\left(\frac{\partial NO_3}{\partial z}\right)$ (mmol m^{-4}) the vertical gradient of nitrate (Sharples et al 2001*b*). During both sampling periods ensembles of 5 – 6 sequential FLY profiles were carried out approximately every hour, with an ensemble taking typically 40 minutes to carry out. Vertical profiles of the CTD (Table 1) were carried out to provide a density-nitrate relation that could then be applied to the FLY density profiles for the calculation of the vertical nitrate gradient through the base of the SCM. A particular advantage of having a reliable density-nitrate relation is that the nitrate gradient and the turbulent diffusivity measurements can then be taken from the same instrument at the same time, avoiding uncertainties associated with separation both in time and space when the diffusivity is measured using FLY and the nitrate gradient is taken from separate CTD casts (e.g., Sharples et al. 2001*b*). Throughout both sampling periods the SCM finished at or just above the σ_t=27.0 kg m^{-3} isopycnal (Fig. 3A, B). The CTD sampling provided sufficient nitrate data to generate a reliable linear density-nitrate regression for each sampling period within the base of the SCM (Fig. 3C, D). This linear density-nitrate relationship allows a combination of Eqs. 1-3 to simplify the estimation of the nitrate flux into the base of the SCM to:

$$NO_{3\,flux} = m\frac{\Gamma\varepsilon\rho}{g} \qquad \text{(mmol } m^{-2}\ s^{-1}\text{)} \qquad (4)$$

with *m* the nitrate-density gradient (mmol m^{-3} (kg m^{-3})$^{-1}$). Because of the vertical movement of the isopycnals associated with the internal tide, nitrate fluxes were calculated at isopycnals rather than isobars. In order for there to be sufficient observations to allow reliable time series through the tidal cycles, the instantaneous fluxes into the base of the SCM were calculated as the average within ±0.1 kg m^{-3} of the 26.8 kg m^{-3} isopycnal (Fig. 3A, B). For both sampling periods this range of 26.7 – 26.9 kg m^{-3} was always situated within the lower SCM. With each FLY profile thus providing a measure of the nitrate flux into the SCM, an ensemble of 5 – 6 FLY profiles then resulted in an ensemble mean nitrate flux with 95% confidence limits calculated using a bootstrapping technique (Efron and Gong 1983). Similarly, a daily mean SCM nitrate flux with confidence intervals was calculated by combining all available flux estimates for sampling period.

Results

Example CTD profiles illustrate the typical temperature, salinity, Chl *a*, and nitrate structure observed during the two sampling periods (Fig. 4A, B), showing a broad SCM reaching from the base of the thermocline towards the surface. During the neap tide sampling period nitrate was consistently just above the detection limit at a depth of 15 m, and below

detection above a depth of 10 m. During the spring tide sampling period nitrate was sometimes detectable at a depth of 2 m.

Comparing the calibrated fluorescence profiles with the chlorophyll samples confirms the existence of an identifiable SCM, though for the neap tide example (Fig. 4A) there is an indication of fluorescence quenching in the upper 10 m that falsely enhances the contrast between the SCM chlorophyll concentration and that at the surface. Both of the examples show significant spiking in the fluorescence-based chlorophyll profiles on vertical scales of 1 – 2 metres (i.e., close to the vertical averaging interval of the CTD data). Such spikes are sometimes thought to be the result of large diatom cells being sampled by the fluorometer. Another possibility is the existence of layers of cells within the SCM. Due to both vessel motion and some difficulties in controlling the CTD winch veer rate, the CTD data was not of a quality to allow high resolution sampling through the SCM. However, there is evidence (Fig. 5) that chlorophyll spikes within the SCM could be consistent between 2 or 3 adjacent CTD casts, possibly associated with small scale structure (i.e. 1 – 5 metres) in the density profile. These layers are perhaps analogous to the thin layers seen in lower turbulence environments (e.g., McManus et al. 2003); their existence is intriguing as they could potentially provide us with some information on the structure of the mixing through the SCM.

The spatial context of this shelf edge temperature, chlorophyll, and nitrate is provided by a cross-shelf edge transect of CTD profiles carried out on 21-22 July (Fig. 6). The structure of the thermocline at the shelf edge was broader than either on-shelf or off-shelf (Fig. 6A), with a reduction of the shelf edge surface temperature by about 1.5°C compared to the adjacent on-shelf and off-shelf waters. This patch of broader thermocline and cooler shelf edge water was coincident with high surface layer chlorophyll (Fig. 6B), comparable to the highest chlorophyll concentrations off-shelf and on-shelf found below the sea surface in the SCM. Similarly the nitracline at the shelf break was broadened (Fig. 6C), with detectable concentrations of nitrate at the sea surface just on-shelf from the 200 m isobath and corresponding with the region of elevated surface chlorophyll concentrations. The corresponding sample analyses of the SCM phytoplankton population showed significant cross-shelf edge contrasts (Fig. 7). Flow cytometer analysis of samples from the peak of the SCM (Fig. 7A) showed a significant change in the proportion of prokaryotes and eukaryotes between the highly stratified waters and the shelf edge region. Prokaryotes, specifically *Prochlorococcus* and *Synechococcus*, dominated in the stratified oceanic and shelf waters respectively. Conversely these oligotrophic organisms were largely absent from shelf edge waters where small eukaryotes instead dominated the picophytoplankton community. Size-fractionated chlorophyll measurements (not shown) indicated that larger eukaryotes were

typically much more abundant at the shelf edge than in oceanic and shelf waters. The >10μm fraction comprised 50-80% of the community at the shelf edge while picoplankton (<2μm) comprised <30%. Conversely on the shelf and in the oceanic waters picoplankton frequently dominated and large (>10μm) eukaryotes rarely accounted for >30% of community chlorophyll. Analysis of the species within one group (the diatoms) showed marked differences across the shelf edge (Fig. 7B). One species (*Leptocylindricus mediterraneus*) was found predominantly on the Atlantic side of the shelf edge, while another (*Pseudonitzschia* sp) was found mainly at the shelf edge and over the shelf. Cells of *Navicula* were only found at the shelf edge. *Rhizosolenia stlyiformis* and *Proboscia alata*, both species that tend to favour stable environments, were absent at the shelf edge.

The longer term context of the variability of the shelf edge water column structure, both during the two occupations of the station and between the two occupations, illustrates the behaviour of the internal tidal motions (Fig. 8). The 12°C isotherm shows a consistent tidal oscillation between neap and spring tides (Fig. 8A), with a typical mid-water peak-to-trough variation of 50 – 60 m. These oscillations sometimes exhibited quite large, bore-like jumps; the four tidal oscillations between noon on 20 July and midnight on 22 July were all associated with marked high-amplitude, high-frequency signals at a depth of 50 m. Extracts from the mooring temperature time series, covering the times of the neap tide and spring tide occupations of the shelf edge site, suggest overall tidal amplitudes of isotherm displacements to be slightly lower during the spring tide sampling period (Fig. 8B, C). At both neap and spring tides the thermocline reached its maximum downward displacement at maximum off-shelf barotropic flow (Fig. 8D, E). While high frequency variability superimposed on the tidal oscillations was a persistent feature of both neap and spring tides, there was a marked contrast in the strength of this higher variability (Fig. 8B, C). There were 20 – 30 minute period oscillations of isotherms in the upper 50 m throughout the neap tide sampling (Fig. 8B), with peak-trough ranges of about 10 m. During the spring tide sampling (Fig. 8C) high frequency wave ranges were typically 20 – 40 m, with particularly strong pulses of waves as the base of the thermocline reached its shallowest depth (e.g., 03:00 h and 15:00 h UTC 23 July, and 03:00 h UTC 24 July).

A strong burst of high frequency internal waves was observed in the mooring time series between 15:00 h and 16:00 h UTC on 23 July (Fig. 8C). At 14:45 h UTC a series of 5 – 6 internal wave bands passing the ship were identifiable on the ship's radar. Tracking one of the waves on the radar, and accounting for the ship's movement, suggested a wave speed of about 0.3 m s^{-1} onto the shelf. The ensemble of FLY profiles that began at 14:16 h UTC was

extended to cover at least 2 or 3 of the waves passing the vessel. The appearance of the waves in the mooring time series after the time of the FLY ensemble and observation on the ship's radar is consistent with the wave travel speed and the cross-shelf distance between the ship and the mooring. This event highlights a problem in sampling the intermittency of wave events apparent in the mooring time series with the sampling resolution of the FLY ensembles. The situation is further complicated when considering that there could be a 0.5 – 2 km distance between the ship and the mooring, so that identifying the timing of FLY ensembles against the mooring time series is not a reliable guide in determining whether or not a high frequency internal wave event was sampled by FLY. We will return to this problem during the discussion in the context of the implications for uncertainties in the nitrate flux calculations when the fluxes appear to be controlled by discrete mixing events.

The observed turbulent dissipation (Fig. 9A, B) shows the expected high dissipation associated with bed friction, with typically an order of magnitude more dissipation at spring tides compared to neap tides consistent with the spring tidal current amplitude being approximately twice that at neaps. During both sampling periods significant turbulent dissipation was also observed in the interior of the water column. At the neap tide (Fig. 9A) this interior dissipation exhibited a tidal periodicity and reached typically 10^{-4} – 10^{-3} m^2 s^{-3} near or below the 27.1 kg m^{-3} isopycnal. Interior dissipation during the spring tide (Fig. 9B) was observed to be generally 1 – 5 x 10^{-4} m^2 s^{-3} close to the 26.9 kg m^{-3} isopycnal, i.e., a slightly lower rate than the neap tide but higher up within the pycnocline and in the base of the SCM.

The supply rate of nitrate to the SCM during the neap tide sampling period (Fig. 9C) ranged between 0.02 and 0.11 mmol m^{-2} h^{-1} and showed no clear tidal oscillation of the nitrate flux. During the spring tide sampling period (Fig. 9D) the flux ranged from 0.02 and 0.74 mmol m^{-2} h^{-1}, dominated by peaks associated with the high dissipation events at the 26.8 kg m^{-3} isopycnal. It is these peaks that are primarily responsible for leading to a higher daily-averaged spring tide nitrate supply to the SCM (3.5 (2.3 – 5.2, 95% confidence interval) mmol m^{-2} d^{-1}) compared to the neap tide daily average (1.3 (0.9 – 1.8, 95% confidence interval) mmol m^{-2} d^{-1}). The daily mean vertical eddy diffusivities (with 95% confidence intervals) within the base of the SCM were 1.2 (0.8 – 1.8) x 10^{-4} m^2 s^{-1} for the neap tide, and 6.5 (3.1 – 10.3) x 10^{-4} m^2 s^{-1} for the spring tide.

Discussion and Conclusions

Observations of the vertical nitrate flux into the base of the SCM at the Celtic Sea shelf edge in summer suggest a difference of a factor of almost 3 between spring tides (3.5

mmol m^{-2} d^{-1}) and neap tides (1.3 mmol m^{-2} d^{-1}). The higher nitrate flux at spring tides resulted from pulses of strong turbulent dissipation occurring within the base of the SCM associated with high frequency internal solitons. During neap tides the highest mid-water turbulent dissipation was observed below the SCM, and high frequency waves were much weaker compared to springs.

Our discussion will focus on three issues. (1) Given the event-based nature of the higher spring tide nitrate flux, can we be sure that we have sampled the flux time series sufficiently to yield a reliable daily flux estimate, and if not can we quantify the likely additional uncertainty? (2) How do the vertical nitrate fluxes and inferred limits on new production compare with other oceanographic environments? (3) What are the consequences of the spring-neap contrast in the vertical nitrate flux for primary productivity at the shelf edge, and does the shelf edge phytoplankton ecosystem respond distinctly to the physical environment compared to the adjacent shelf and open ocean?

In addressing whether or not we adequately sampled the flux time series we can take advantage of having the rapid-sampling temperature time series from the mooring adjacent to the ship's station at the shelf edge. During the spring tide the mooring data (Fig. 8C) suggests that particularly strong pulses of internal wave activity within the SCM occurred periodically every tidal cycle. Also, the largest nitrate flux estimate (at about 19:30 h UTC on 23 July, Fig. 9D) appeared to coincide with the passage of a single large soliton (Fig. 8C). Thus, while the FLY sampling of turbulent dissipation illustrated in Fig. 8C may be sufficient to yield a reliable daily mean flux estimate if the flux varies smoothly over a tidal cycle, the dominance of these short-lived mixing events suggests that instead we need to consider the possibility that we missed some of them. For instance, we know that we were only able to sample just under half of the packet of internal waves observed on the ships radar during the spring tide sampling period. Similarly there are internal wave events evident in the mooring time series that are not reflected in the flux time series, suggesting that FLY did not adequately sample them (e.g., 03:00 h UTC, 12:30 h UTC, and 13:30 h UTC on 23 July; Fig. 8C). Of the 25 hours occupation of the station during the spring tide, FLY profiles were carried out for a total of 9.4 hours, or 38% of the time. Assuming that there was sufficient variability in the timing of the FLY profiles over the 2 tidal cycles (i.e., measurements were not in phase with the tidal variability), then 38% of the mixing events were sampled with FLY. If these events dominate the daily flux estimate, ideally sampling all of the events could raise the daily averaged spring tide nitrate flux to about 9 mmol m^{-2} d^{-1}. A similar analysis for the neap tide sampling period raises the neap tide daily mean nitrate flux to about 4 mmol m^{-2} d^{-1}. However, in the case of the neap tide it is far less apparent from either the FLY time series (Fig. 9C) or the mooring

time series (Fig. 8B) that the nitrate flux was determined by isolated, discreet events. Thus the original estimate of 1.3 mmol m^{-2} d^{-1} is likely to be a better reflection of the true neap tide nitrate supply to the SCM.

The observed stronger thermocline mixing and vertical nitrate flux at spring tide, compared to neaps, agrees with previous work that has shown the importance of spring tides for internal mixing at the Celtic Sea shelf edge (New and Pingree 1990). The increased internal mixing at spring tides is probably the reason for the similar internal tidal wave amplitudes observed at neap and spring tides, with more energy having been dissipated from the internal tide at springs. The contrast between the spring tide, with vertical fluxes being driven by events of internal solitons, and neap tides where little soliton activity was observed, is consistent with previous observations (Pingree and Mardell 1985) and numerical modelling of the region (Gerkema 1996). The difference in sea level range between the neap and spring sampling periods in this study was typical for the large neap-spring changes in the region (Fig. 2B), indicating that there could be a marked spring-neap cycle in vertical nitrate flux as a result of the spring tide solitons. However, spring tides on 8 July and 8 August were substantially weaker than the spring tide sampled on 23/24 July, and we have no evidence that solitons would have been generated at these weaker spring tides. It is therefore possible that the strong monthly modulation of the strength of spring tides may mean that the vertical nitrate flux is pulsed on a monthly rather than fortnightly time scale.

The neap tide estimate of vertical flux of nitrate at the shelf edge of the Celtic Sea is similar to flux measurements made in a strongly-stratified water column in the western English Channel (Sharples et al. 2001*b*). There the daily mean flux of about 2 mmol m^{-2} d^{-1} was thought to be the result of tidally-driven boundary turbulence impacting the base of the thermocline, rather than internal waves. Vertical nitrate fluxes comparable to spring tides at the Celtic Sea shelf edge have also been found within the tidal mixing front off Georges Bank (Horne et al. 1996), where primary production rates were also seen to be enhanced compared to waters on either side of the front.

Without taking into account the potential for under sampling of mixing events during spring tides, the spring tide daily mean diffusivity in the base of the SCM at the Celtic Sea shelf edge (6.5×10^{-4} m^2 s^{-1}) is similar to that measured in an internal tide dominated environment at the shelf edge of NE New Zealand (Sharples et al. 2001*a*). The weaker nitrate flux at the Celtic Sea shelf edge (3.5 mmol m^{-2} d^{-1} compared to 12 mmol m^{-2} d^{-1} off New Zealand) is a result of lower sub-thermocline nitrate concentrations and a subsequently lower vertical nitrate gradient. Taking into account the event-driven nature of the internal tide-

driven nitrate flux in the Celtic Sea does bring the flux estimate closer to that of NE New Zealand. However, if vertical fluxes driven by non-linear internal tides are dominated by mixing events associated with the passage of solitons, the NE New Zealand fluxes could also be under-estimated.

Assessing the potential importance of the vertical nitrate flux to enhancing new production at the shelf edge needs to start with an estimate of how much production can be maintained by the fluxes. Phytoplankton C:N ratios tend, on average, to be close to the Redfield ratio, but can vary both through time and between groups (e.g., Geider and La Roche 2002). If we assume phytoplankton growth maintains an approximate C:N Redfield ratio of 6.6, then the neap tide vertical flux of nitrate could support new carbon fixation of 120 mg C m^{-2} d^{-1}. At spring tides the increased nitrate flux could support enhanced new production of between 320 and 830 mg C m^{-2} d^{-1}, with the higher rate taking into account under-sampling of the mixing events. Water column estimates of primary production during the OMEX project (Joint et al. 2001) show rates in July to be typically 400 mg C m^{-2} d^{-1}, with a quarter of that being fuelled by nitrate from below the thermocline. This earlier estimate is consistent with our neap tide nitrate flux, but would imply that our observed spring tide nitrate flux is in excess of the monthly-mean nitrate uptake capacity.

Further insight into the behaviour of the primary production can be gained by considering the measured nitrate fluxes alongside the detailed observations of primary production. At neap tides the capacity for carbon fixation between the base of the SCM and the sea surface was estimated to range between 370 and 800 mg C m^{-2} d^{-1}, with the range based on the cloudiest and sunniest days experienced during the cruise. This suggests that all of the neap tide daily mean nitrate supply could be utilised by the phytoplankton, with an *f*-ratio of between 0.14 and 0.32. With the reasonable assumption that the nitrate flux will not change with surface irradiance this implies that the use of locally regenerated nitrogen would have to be increased on sunny days.

The observed carbon fixation capacity at spring tides was slightly less than that at neaps, ranging between 290 and 600 mg C m^{-2} d^{-1}, reflecting a lower chlorophyll standing stock and indicating potential acclimation to the more stable light environment at neap tides. Using the original estimate of the spring nitrate flux this would suggest an *f*-ratio between 0.5 and 1. Taking into account the likely underestimate of the nitrate flux due to under-sampling of mixing events would imply that the supply of nitrate was well in excess of phytoplankton nitrogen requirements at spring tides. This inability of the phytoplankton population to take up the supplied nitrate at spring tide is supported by the observation of nitrate in the surface

samples during the spring tide sampling period, and by the generally higher spring tide surface layer nitrate implied by the temperature-nitrate relationships for the two sampling periods (Fig. 3C, D). The phytoplankton community thus appears to require a few days to take up the available nitrate and utilise it, and to reduce the surface layer nitrate back to neap tide values. A simple model illustrates this proposed mechanism whereby the build-up of chlorophyll in response to the spring-neap cycle in vertical nitrate flux lags the peak flux. Using the upper (spring tide) and lower (neap tide) limits of nitrate fluxes observed, the nitrate flux to the surface layer is described as

$$NO_{3\,flux} = 5.15 + 2.85 \sin\left(\omega_{SN} t\right) \quad \text{(mmol m}^{-2}\text{ d}^{-1}\text{)} \qquad (5)$$

with ω_{SN} = 0.425 d^{-1} the spring-neap angular frequency and t (d) is time. The model assumes that the nitrate flux is all instantly converted into increased phytoplankton biomass (Chl *a*) within the surface layer using a fixed ratio of 1.59 g Chl *a* (mol N)$^{-1}$ (Platt et al. 2003), and that grazing and other loss terms balance the supply of nitrate over the full spring-neap cycle:

$$\left(\frac{\partial Chl}{\partial t}\right) = \frac{1.59 NO_{3\,flux}}{MLD} - G \qquad \text{(mg m}^{-3}\text{ d}^{-1}\text{)} \qquad (6)$$

The surface layer was taken to be MLD = 40 metres, and the loss term G = 0.2 d^{-1} in order to balance the growth over the spring neap cycle. A minimum "background" chlorophyll concentration was set at 0.9 mg m^{-3}. In the simple case presented (Fig. 10) the build-up of pigment lags the maximal flux by ~3.5 days. This is consistent with an estimate of the phytoplankton carbon turnover rate. With a mean standing stock of about 2 g C m^{-2} in the upper 40 m (taking a mean Chl *a* stock of 50 mg Chl m^{-2} and assuming C:Chl≈40), and a measured typical growth rate of 0.5 g C m^{-2} d^{-1}, leads to a carbon turnover rate of 4 days.

This slow growth response, which potentially arises from light limitation driven by the internal mixing, could allow the build-up of surface nitrate. If the upper ocean system is capable of storing this excess nitrate, the unutilized nitrate supply driven during the spring tides could then provide fuel for later growth during increased stability towards the next neap tide, leading to further delay in growth and a peak standing stock in the surface waters several days after spring tides. Approaching the next spring tide would then not only begin the re-supply of nitrate, but would also remove some of the biomass into the deeper water below the SCM. This implies a potential for fortnightly pulsing of primary production at the shelf edge (or monthly, if weaker spring tides generate fewer internal solitons), with the biomass lagging

the supply of nitrate. The extent of this pulsed response to nitrate mixing would also be modulated by the available light.

The suggested mechanism for a delayed growth response to spring tide nitrate fluxes arises from our observations of neap-spring contrasts in vertical mixing and nitrate fluxes, coupled with the measurements of primary production. While the observed higher surface water nitrate at spring tides and the higher neap tide surface biomass are consistent with this mechanism, our observations are not sufficient to rule out other reasons for the neap-spring contrasts in surface nitrate and biomass. One obvious alternative in this region of significant along-slope flows (e.g., Huthnance et al. 2001) is simply the advection of different water properties into the region between the two sampling periods. Further investigation would require an understanding of the along-shelf edge gradients, and would benefit from the use of a coupled numerical model of the shelf edge and internal tide.

In addition to the mixing environment increasing new primary production at the shelf edge (Joint et al. 2001), this narrow, physically distinct region is also associated with a marked shift in phytoplankton community structure compared to the adjacent Celtic Sea and NE Atlantic Ocean (Fig. 7). Overall the larger eukaryotes dominated the shelf edge, compared to picoplankton dominance on and off the shelf. Within the eukaryotes there was also a change in species across the shelf edge, with species generally associated with stable environments absent from the region of internal tide mixing. Thus the gradient of physical processes from the shelf, across the shelf edge, and into the open Atlantic is associated with significant changes in the community structure of the phytoplankton, and the vertical internal mixing at the shelf edge is not simply redistributing an otherwise horizontally uniform population of cells. Rather the stronger mixing and the resultant upward flux of nutrients results in a shift in community structure from prokaryote domination on and off shelf to a greater proportion of eukaryotes and larger cells at the shelf edge. Such an increase in community size structure is typical of enhanced nutrient availability (Chisholm 1992).

In summary, we have quantified a spring-neap contrast in the vertical flux of nitrate to the SCM at the shelf edge of the Celtic Sea in summer. The larger flux during the spring tide is a result of the internal turbulent dissipation occurring within the base of the SCM, rather than any overall increase in internal turbulence compared to neap tides, and was dominated by short mixing events. A simple assessment of the implications of the flux dependence on these short events leads to a substantial increase in the estimate of the spring tide vertical nitrate flux. The shelf edge new production supportable by the observed neap tide nitrate fluxes is consistent with both earlier work and with primary productivity

measurements made during the flux estimates. During spring tides, however, nitrate fluxes were likely to be in excess of the capacity of the primary producers to utilise it instantaneously; we suggest that this could lead to a fortnightly cycle of nitrate supply during spring tides followed by utilisation and growth towards neaps. We have also provided evidence for a link between the gradients in physical processes across the shelf edge and changes in the community structure of the phytoplankton at both group and species levels. An interesting (and ambitious) topic for further research would be to understand the physiological mechanisms behind the changes in community structure, and to assess them in the context of the productivity at higher trophic levels often seen in the shelf edge ecosystem.

References

BAINES, P.G. 1982. On internal tide generation models. Deep-Sea Research **29:** 307-338.

BEZ, N., AND J. RIVOIRARD. 2001. Transitive geostatistics to characterise spatial aggregations with diffuse limits: an application on mackerel ichtyoplankton. Fisheries Research **50:** 41-58.

BRICKMAN D., AND J. W. LODER. 1993. Energetics of the internal tide on northern Georges Bank. Journal of Physical Oceanography **23:** 409-424.

CHISHOLM, S. W. 1992. Phytoplankton size, p. 213-273. *In* P.G. Falkowski and A. Woodhead [eds.], Primary Productivity and Biogeochemical Cycles in the Sea. Plenum.

DALE, A. C., D. S. ULLMAN, J. A. BARTH, AND D. HEBERT. 2003. The front on the northern flank of Georges Bank in spring: 1. Tidal and subtidal variability. Journal of Geophysical Research **108**, citation number, doi:10.1029/2002JC001327

DEWEY, R. K., A. E. GARGETT, AND N. S. OAKEY. 1987. A microstructure instrument for profiling oceanic turbulence in coastal bottom boundary layers. Journal of Atmospheric and Oceanic Technology **4:** 288-297.

EFRON, B., AND G. GONG. 1983. A leisurely look at the bootstrap, the jack-knife and cross-validation. Am. Stat. **37:** 36-48.

ELSKENS M, W. BAEYENS, AND L. GOEYENS. 1997. Contribution of nitrate to the uptake of nitrogen by phytoplankton in an ocean margin environment. Hydrobiologia **353:** 139-152.

FERNANDEZ, E., J. CABAL, J. L. ACUNA, A. BODE, A. BOTAS, AND C. GARCIASOTO. 1993. Plankton distribution across a slope-current induced front in the southern Bay of Biscay. Journal of Plankton Research **15:** 619-641.

GARRETT, C. 2003. Internal Tides and Ocean Mixing. Science **301:** 1858-1859.

GEIDER, R. J., AND J. LA ROCHE. 2002. Redfield revisited: variability of C:N:P in marine microalgae and its biochemical basis. European Journal of Phycology **37:** 1-17.

GERKAMA, T. 1996. A unified model for the generation and fission of internal tides in a rotating ocean. Journal of Marine Research **54**: 421-450.

GRASSHOFF, K. M., K. M. ERHARDT, AND K. KREMLING. 1983. Methods of seawater analysis. Verlag-Chemie.

HEATHERSHAW, A. D., A. L. NEW, AND P. D. EDWARDS. 1987. Internal tides and sediment transport at the shelf break in the Celtic Sea. Continental Shelf Research **7:** 485-517.

HOLLIGAN, P. M., R. D. PINGREE, AND G. T. MARDELL. 1985. Oceanic solitons, nutrient pulses and phytoplankton growth. Nature **314:** 348-350.

HOLLOWAY, P.E., P. G. CHATWIN, AND P. CRAIG. 2001. Internal Tide Observations from the Australian North West Shelf in Summer 1995. Journal of Physical Oceanography **31:** 1182-1199.

HORNE, E. P. W., J. W. LODER, C. E. NAMIE, AND N. S. OAKEY. 1996. Turbulence dissipation rates and nitrate supply in the upper water column on Georges Bank. Deep-Sea Research II **43:** 1683–1712.

HUTHNANCE, J.M. 1995. Circulation, exchange and water masses at the ocean margin: The role of physical processes at the shelf edge. Progress in Oceanography **35:** 353-431.

HUTHNANCE, J. M., H. COELHO, C. R. GRIFFITHS, P. J. KNIGHT, A. P. REES, B. SINHA, A. VANGRIESHEIM, M. WHITE, AND P. G. CHATWIN. 2001. Physical structures, advection and mixing in the region of Goban spur. Deep-Sea Research II **48:** 2979-3021.

INALL, M.E., G. I. SHAPIRO, AND T. J. SHERWIN. 2001. Mass transport by non-linear internal waves on the Malin Shelf. Continental Shelf Research **21:** 1449-1472.

JOINT, I., R. WOLLAST, L. CHOU, S. BATTEN, M. ELSKENS, E. EDWARDS, A. HIRST, P. BURKILL, S. GROOM, S. GIBB, A. MILLER, D. HYDES, F. DEHAIRS, A. ANTIA, R. BARLOW, A. REES, A. POMROY, U. BROCKMANN, D. CUMMINGS, R. LAMPITT, M. LOIJENS, F. MANTOURA, P. MILLER, T. RAABE, X. ALVAREZ-SALGADO, C. STELFOX, AND J. WOOLFENDEN. 2001. Pelagic production at the Celtic Sea shelf break. Deep-Sea Research II **48:** 3049-3081.

LIU, K.K., K. ISEKI AND S. –Y. CHAO. 2000. Continental margin carbon fluxes, p. 187-239. *In* R. B. Hanson, H. W. Ducklow, and J. G. Field [eds.], The Changing Ocean Carbon Cycle. Cambridge University Press.

LORENZO, L. M., F. G. FIGUEIRAS, G. H. TILSTONE, B. ARBONES AND, L. MIRON. 2004. Photosynthesis and light regime in the Azores Front region during summer: are light-saturated computations of primary production sufficient? Deep-Sea Research I **51:** 1229-1244.

MCMANUS M. A., A. L. ALLDREDGE, A. H. BARNARD, E. BOSS, J. F. CASE, T. J. COWLES, P. L. DONAGHAY, L. B. EISNER, D. J. GIFFORD, C. F. GREENLAW, C. M. HERREN, D. V. HOLLIDAY, D. JOHNSON, S. MACINTYRE, D. M. MCGEHEE, T. R. OSBORN, M. J. PERRY, R. E. PIEPER, J. E. B. RINES, D. C. SMITH, J. M. SULLIVAN, M. K. TALBOT, M. S. TWARDOWSKI, A. WEIDEMANN, AND J. R. ZANEVELD. 2003. Characteristics, distribution and persistence of thin layers over a 48 hour period. Marine Ecology Progress Series **261:** 1-19.

MOORE, C. M., D. J. SUGGETT, A. E. HICKMAN, Y. –N. KIM, J. F. TWEDDLE, J. SHARPLES, R. J. GEIDER, AND P. M. HOLLIGAN. 2006. Phytoplankton photoacclimation and photoadaptation in response to environmental gradients in a shelf sea. Limnology and Oceanography **51:** 936-949.

NEW, A. L. 1988. Internal tidal mixing in the Bay of Biscay. Deep-Sea Research A **35:** 691-709.

NEW, A. L., AND R. D. PINGREE. 1990. Evidence for internal tidal mixing near the shelf break in the Bay of Biscay. Deep-Sea Research A **37:** 1783-1803.

OSBORN, T. R. 1980. Estimates of the local rate of vertical diffusion from dissipation measurements. Journal of Physical Oceanography **10:** 83–89.

PINGREE, R. D., D. K. GRIFFITHS, AND G. T. MARDELL. 1984. The structure of the internal tide at the Celtic Sea shelf break. Journal of the Marine Biological Association of the UK **64:** 99-113.

PINGREE, R.D., AND G.T. MARDELL. 1981. Slope turbulence, internal waves and phytoplankton growth at the Celtic Sea shelf-break. Phil. Trans. R. Soc. Lond. **A302:** 663–682.

PINGREE, R.D., AND G.T. MARDELL. 1985. Solitary internal waves in the Celtic Sea. Progress in Oceanography **14:** 431-441.

PLATT T., S. SATHYENDRANATH, A. M. EDWARDS, D. S. BROOMHEAD, AND O. ULLOA. 2003. Nitrate supply and demand in the mixed layer of the ocean. Marine Ecology Progress Series **254:** 3-9.

PUIG P., A. PALANQUES, J. GUILLÉN, AND M. EL KHATAB. 2004. Role of internal waves in the generation of nepheloid layers on the northwestern Alboran slope: Implications for continental margin shaping. Journal of Geophysical Research **109**, citation number, doi:10.1029/2004JC002394.

REID, D. G. 2001. SEFOS - shelf edge fisheries and oceanography studies: an overview. Fisheries Research **50:** 1-15.

RIPPETH, T. P., AND M. E. INALL. 2002. Observations of the internal tide and associated mixing across the Malin Shelf. Journal of Geophysical Research **107**, citation number, doi:10.1029/2000JC000761.

RIPPETH, T. P., J. H. SIMPSON, E. WILLIAMS, AND M. E. INALL. 2003. Measurement of the rates of production and dissipation of turbulent kinetic energy in an energetic tidal flow: Red Wharf Bay revisited. Journal of Physical Oceanography **33:** 1889-1901.

SHARPLES, J., C. M. MOORE, AND E. R. ABRAHAM. 2001*a*. Internal tide dissipation, mixing, and vertical nitrate flux at the shelf edge of NE New Zealand. Journal of Geophysical Research **106:** 14,069-14,081.

SHARPLES, J., C. M. MOORE, T. P. RIPPETH, P. M. HOLLIGAN, D. J. HYDES, N. R. FISHER, AND J. H. SIMPSON. 2001*b*. Phytoplankton distribution and survival in the thermocline. Limnology and Oceanography **46:** 486-496.

WELSCHMEYER, N. A. 1994. Fluorometric analysis of chlorophyll *a* in the presence of chlorophyll-*b* and pheopigments. Limnology and Oceanography **39:** 1985-1992.

WISHNER, K., E. DURBIN, A. DURBIN, M. MACCAULAY, H. WINN, AND R. KENNEY. 1988. Copepod patches and Right Whales in the Great South Channel off New England. Bulletin of Marine Science **43**: 825-844.

YOUNG, J.W., R. BRADFORD, T. D. LAMB, L. A. CLEMENTSON, R. KLOSER, AND H. GALEA. 2001. Yellowfin tuna (*Thunnus albacares*) aggregations along the shelf break off southeastern Australia: links between inshore and offshore processes. Marine and Freshwater Research **52:** 463-474.

Table Captions.

Table 1.

Times of the CTD casts and depths of water sampling during the neap and spring tide sampling stations. All sample depths were analysed for nitrate; underlined sample depths were also sampled for Chl *a*.

Figure Captions.

Figure 1.

A schematic illustration of the generation and dissipation of the internal tidal wave. (A) During off-shelf ebb barotropic tidal flow the thermocline is depressed over the shelf edge and upper slope, forming the main internal tidal wave (wavelength typically 10 – 30 km). (B) As the ebb tidal flow decreases this internal tidal wave propagates both on- and off-shelf, forming shorter internal waves; the short internal waves that cross the shelf edge towards the shallower shelf water can steepen and increase in amplitude. (C) During the early the flood tide the train of internal solitary waves can further shorten (typically to ~ 1km) and steepen in the shallower shelf water, leading to high current shear and subsequent localised vertical mixing as the waves quickly dissipate. The amplitude of the initial internal tidal wave, and the potential for it to dissipate on the shelf via internal solitary waves, is strongly dependent on the strength of the barotropic tidal currents. The arrows indicate the direction and strength of the barotropic tidal currents. [Based on the results of Gerkama 1996 relevant to a spring tide at the Celtic Sea shelf edge].

Figure 2.

(A) Location map of the Celtic Sea and (B) the monthly variability in the strength of the tide illustrated by the tidal range at Falmouth (grey dot in panel A). The box in panel A indicates the area covered by satellite images of (C) sea surface temperature and (D) sea surface chlorophyll. In panels C and D the white circle at the shelf edge is the position of the site of the neap and spring tide sampling periods. The line across the shelf edge is the location of the CTD transect. Satellite images (AVHRR and MODIS) are composites for 11 – 13 July 2005, courtesy of the Remote Sensing Data Analysis Service, Plymouth Marine Laboratory.

Figure 3.

Distribution of Chl *a* measurements against σ_t for all CTD casts during (A) the neap tide sampling period and (B) the spring tide sampling period, and the nitrate-σ_t relationship within the lower half of the SCM for all nitrate samples collected during (C) the neap tide sampling period and (D) the spring tide sampling period. The grey region in panels A and B indicates the σ_t limits through which the nitrate fluxes into the base of the SCM are calculated. The slopes, *m*, of the linear regressions in panels C and D are used in Equation 4. The dashed line in panel D is the neap tide regression repeated from panel C, indicating the increase in nitrate throughout the SCM during spring tides.

Figure 4.

Example CTD cast data from (A) 07:20 h UTC 18 July during the neap tide sampling period, and (B) 04:00 h UTC 24 July during the spring tide sampling period.

Figure 5.

An example of the coherence of spikes in the fluorescence-derived vertical profiles of chlorophyll across 3 of the spring tide CTDs. The horizontal dashed line joins the same chlorophyll spike based on a constant σ_t.

Figure 6.

Cross shelf edge CTD transect (A) temperature, (B) Chl *a*, and (C) nitrate, carried out between 20:25 h UTC 21 July and 21:30 h UTC 22 July. See Fig. 2 for the location of the transect line. CTD positions are shown by the vertical lines in panels A and B. Circles in panel C show the positions of the nitrate samples. Numbers along the top of panel A refer to CTD casts.

Figure 7.

Results from the phytoplankton samples collected in the cross-shelf edge transect of CTD stations. (A) Cell concentrations for *Prochlorococcus*, *Synechococcus*, and picoeukaryotes measured using a flow cytometer, and (B) Cell concentrations for the diatom species observed, expressed as a percentage of the transect average of each species. CTD station numbers correspond to those marked in Fig. 6A. The "stable water" species in panel B are *Rhizosolenia styliformis* and *Proboscia alata*. Samples were collected from the peak of the SCM. Comparison with other samples from within the SCM did not indicate any significant vertical variations in community structure.

Figure 8.

Variations in the vertical temperature structure between neap and spring tides, recorded by the moored temperature loggers for (A) the whole mooring deployment, (B) the neap tide sampling period, and (C) the spring tide sampling period; the shaded bars indicate the times during which FLY ensembles were conducted. Depth-averaged cross-shelf velocities are shown for (D) the neap and (E) the spring sampling periods; positive flow is on-shelf.

Figure 9.

Time series of turbulent dissipation (colours) and σ_t (lines) for (A) the neap tide sampling period and (B) the spring tide sampling period. Turbulent dissipation is ensemble averaged, with the mean time of the FLY ensembles indicated by the vertical lines. Isopycnals are shown every 0.2 kg m^{-3}. (C) and (D) are the time series of the vertical nitrate fluxes through the base of the thermocline during the neap and spring tide sampling periods respectively; in each case the flux was calculated between the dashed contours shown in panels A and B. Vertical bars in panels C and D are 95% confidence intervals. Note that the gap at the start of the spring time series panels B and D results from having only one successful FLY profile at the start of the sampling period, which could not be used to estimate a mean dissipation and flux.

Figure 10.

Results of the simple model (Eq. 6) linking a spring-neap (A) cycle in nitrate flux to a (B) cycle in chlorophyll biomass, illustrating the lag of biomass behind the nitrate supply. In panel A the circles are the nitrate flux observations used to set the limits of the spring-neap flux time series used by the model. In panel B the circles are the mean surface layer chlorophyll concentrations averaged over all CTD casts during the two sampling period. The error bars in panel B are ± one standard deviation of the sampling period averages.

Sampling period	CTD times (UTC)	Sample depths (m)
17/18 July	18:57 h 17 July	2, 15, 25, 35, 43, 60, 75, 100, 125, 150, 175
	07:20 h 18 July	2, 5, 10, 15, 25, 30, 35, 40, 45, 50, 60, 80, 100, 120, 140, 160, 180, 200
	12:02 h 18 July	2, 20, 40, 60, 70, 80, 100, 120, 140, 160, 180, 200
	18:39 h 18 July	2, 15, 25, 40, 50, 60, 70, 90, 110, 130, 150, 170
23/24 July	03:00 h 23 July	2, 10, 20, 30, 40, 50, 60, 70, 80, 90, 100, 120, 140, 160, 180
	10:32 h 23 July	2, 10, 30, 60, 80
	15:25 h 23 July	2, 10, 20, 30, 40, 50, 60, 80, 100, 120, 140, 160, 175
		2, 20, 40, 60, 80
	20:00 h 23 July	2, 20, 40, 60, 80
	23:07 h 23 July	2, 10, 20, 30, 40, 50, 60, 80, 100, 120, 155
	04:04 h 24 July	

TABLE 1

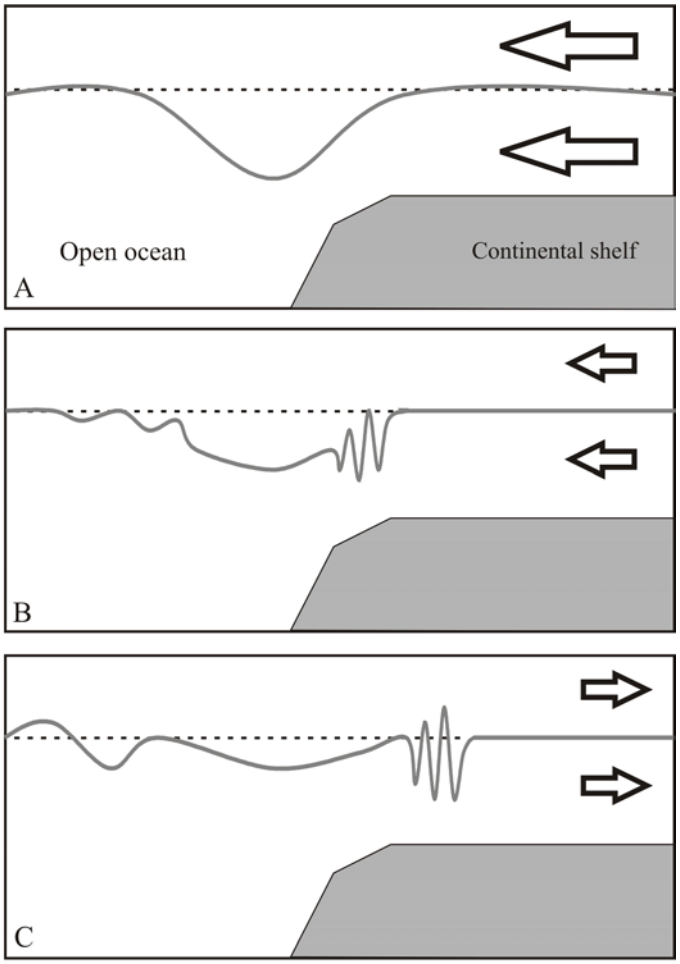

06-560 Figure 1

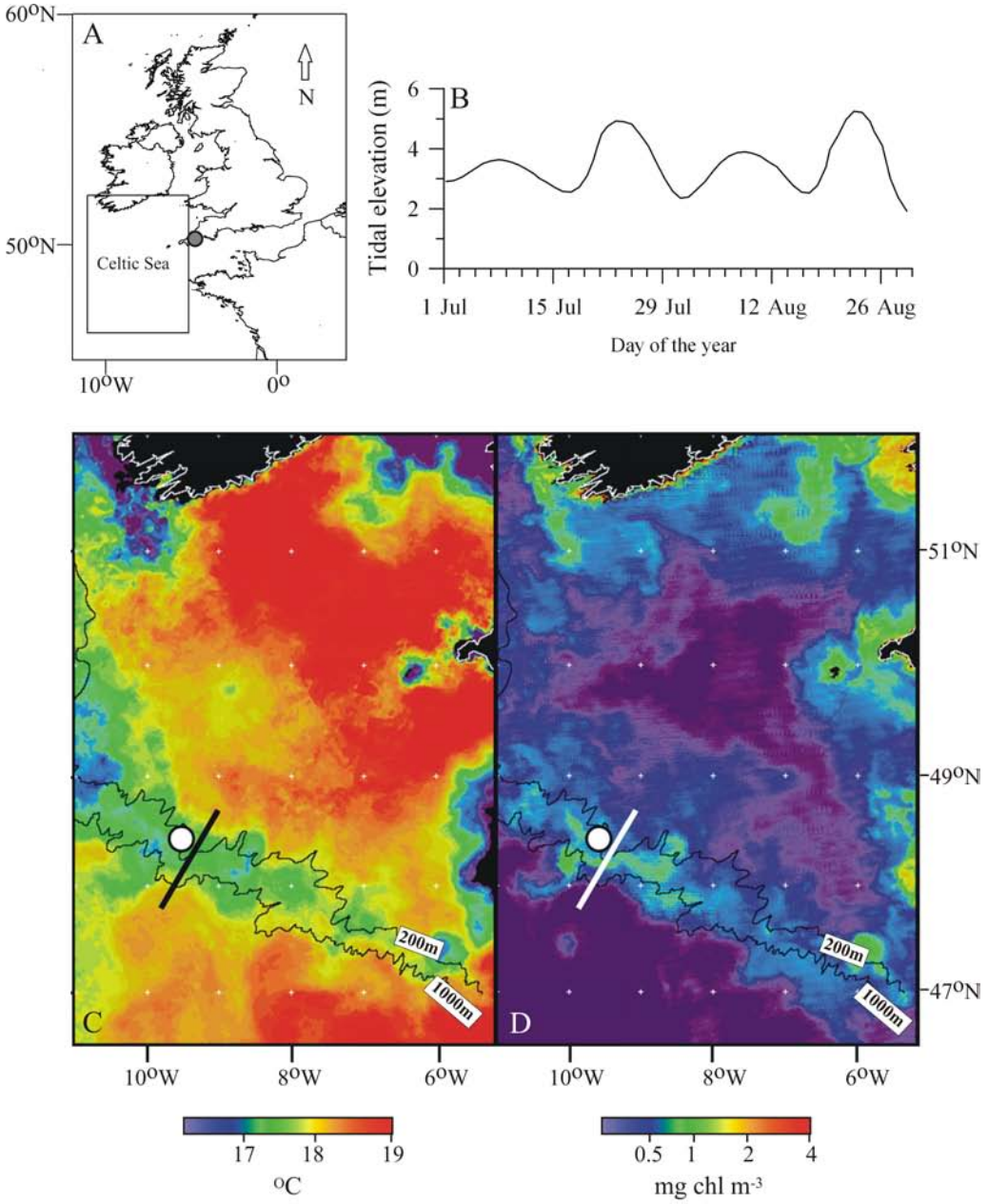

06-560 Figure 2

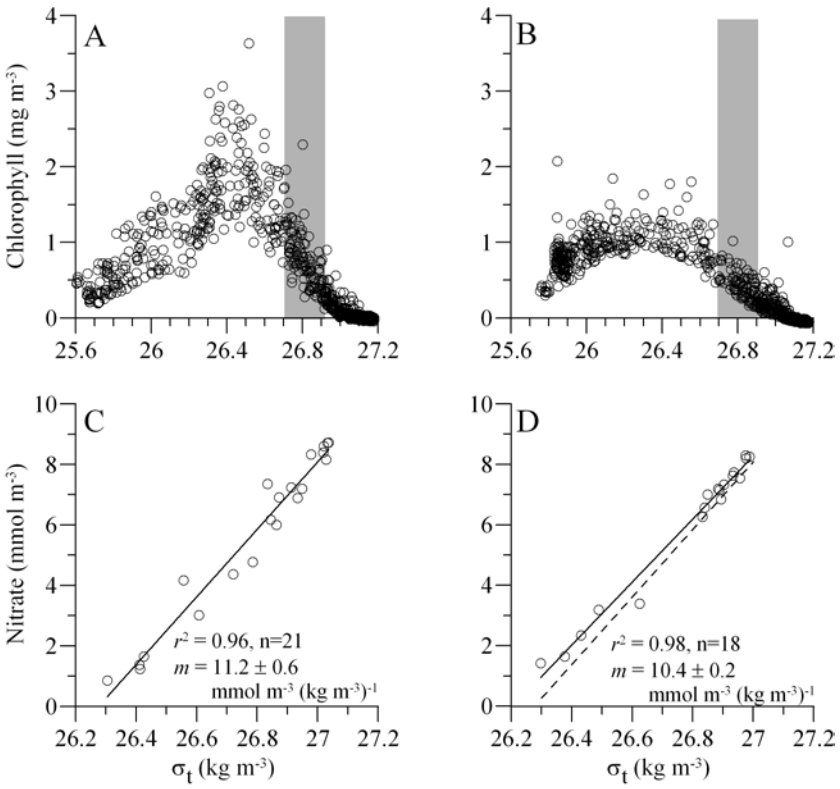

06-560 Figure 3

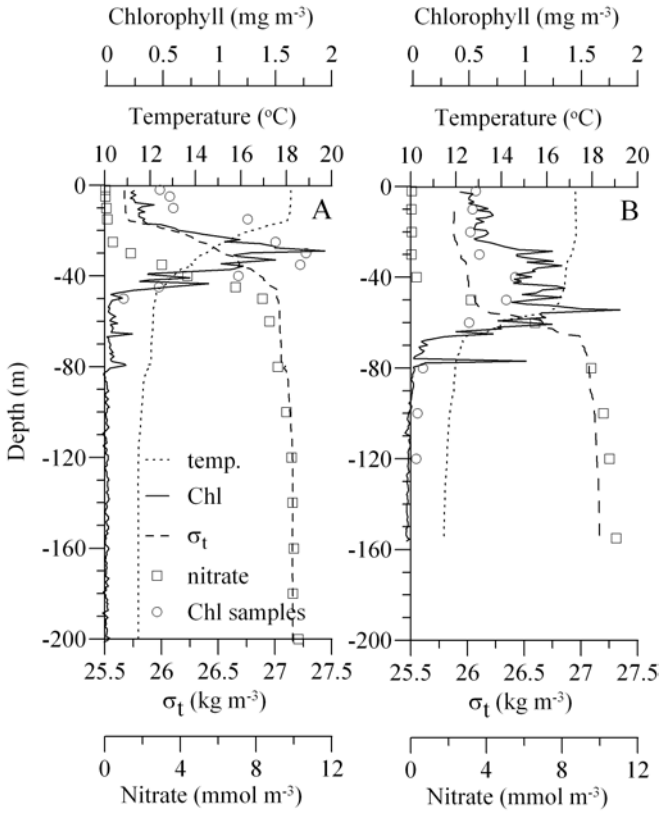

06-560 Figure 4

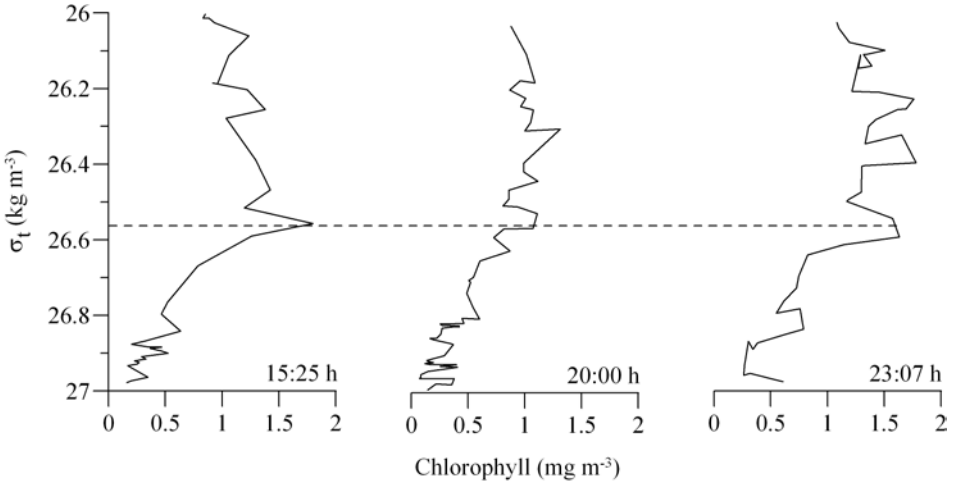

06-560 Figure 5

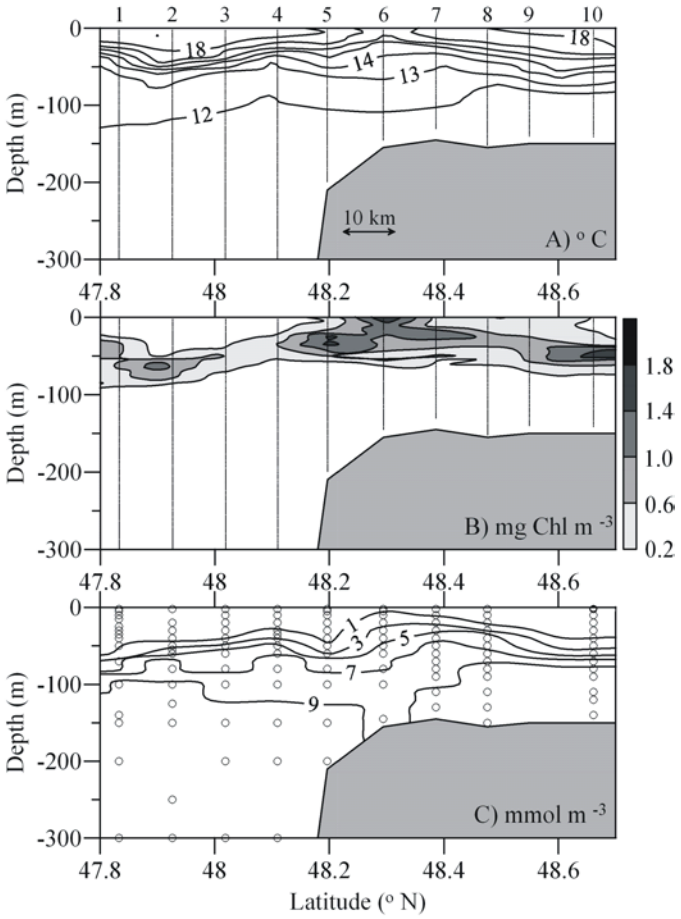

06-560 Figure 6

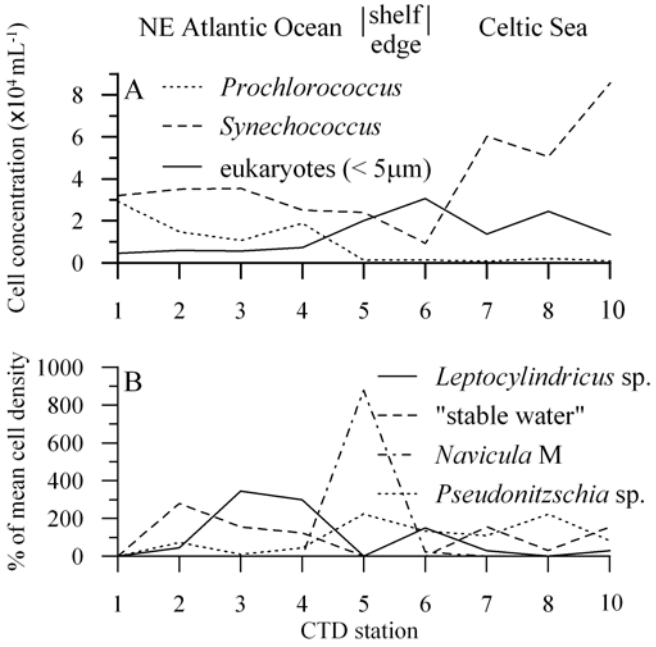

06-560 Figure 7

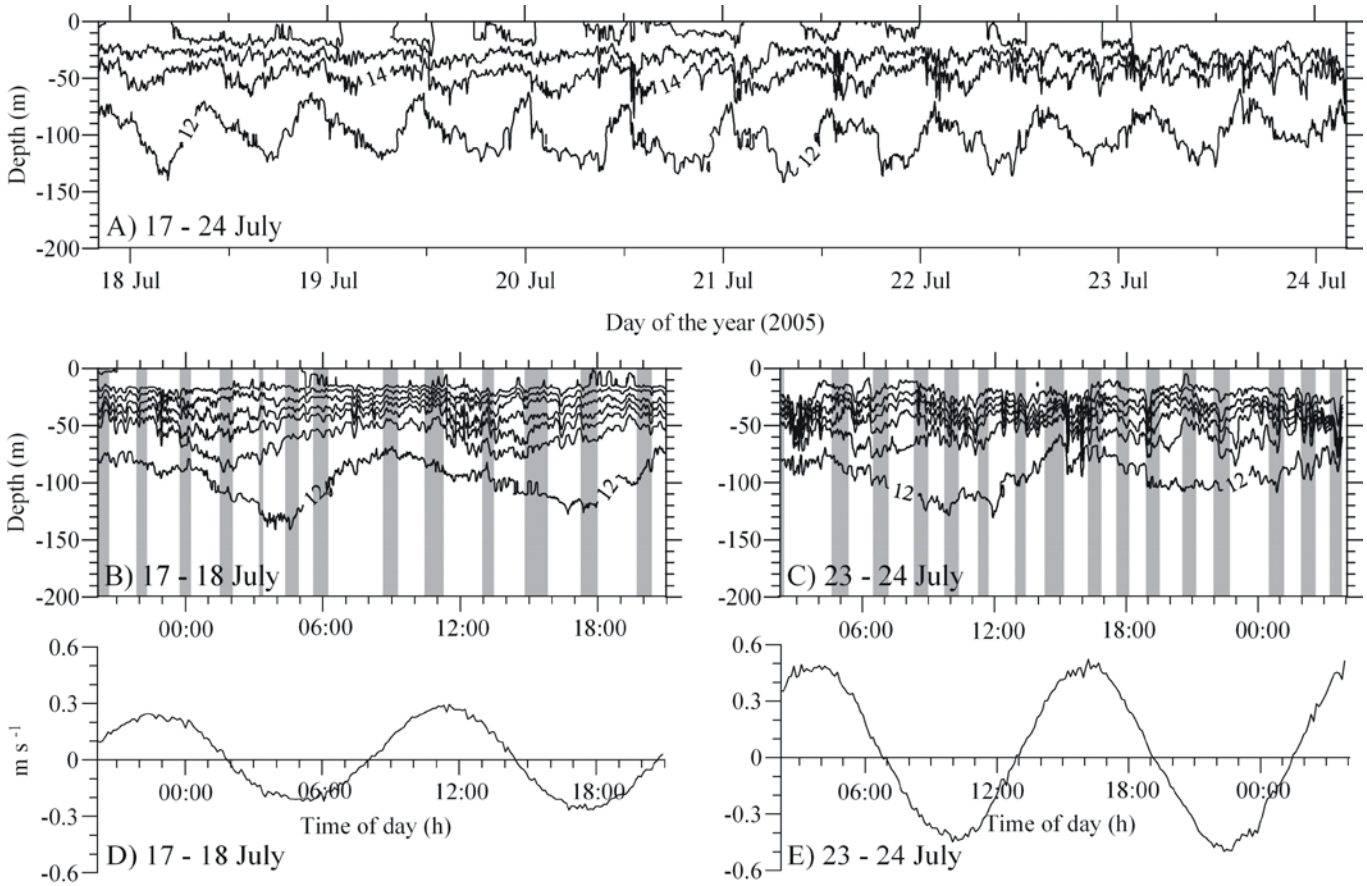

06-560 Figure 8

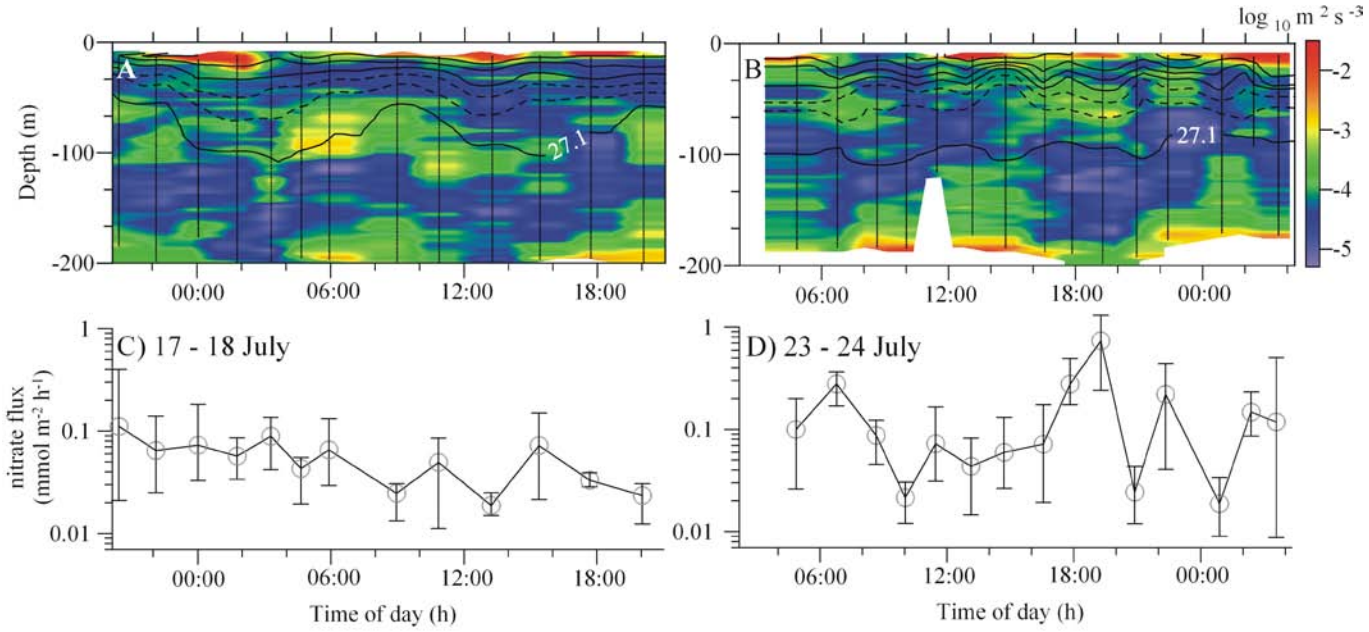

06-560 Figure 9

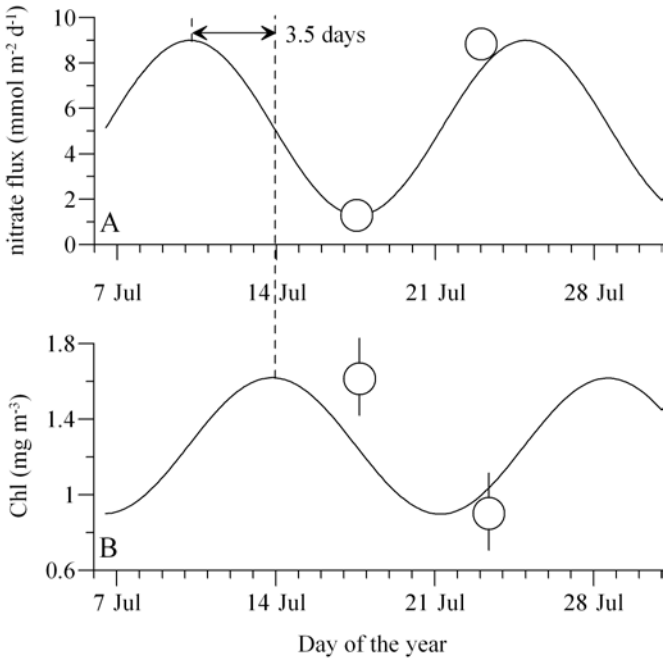

06-560 Figure 10